

SYNOVIAL FLUID PROFILE DICTATES NANOPARTICLE UPTAKE INTO CARTILAGE- IMPLICATIONS OF THE PROTEIN CORONA FOR NOVEL ARTHRITIS TREATMENTS

*Ula von Mentzer¹, Tilia Selldén¹, Loise Råberg¹, Gizem Erensoy¹, Anna-Karin Hultgård-Ekwall^{2,3},
Alexandra Stubelius^{1,*}*

*¹Division of Chemical Biology, Department of Biology and Biological Engineering, Chalmers
University of Technology, Gothenburg, Sweden.*

²The Rheumatology Clinic, Sahlgrenska University Hospital, Gothenburg, Sweden.

*³Department of Rheumatology and Inflammation Research, Institute of Medicine, Sahlgrenska
Academy of University of Gothenburg, Gothenburg, Sweden.*

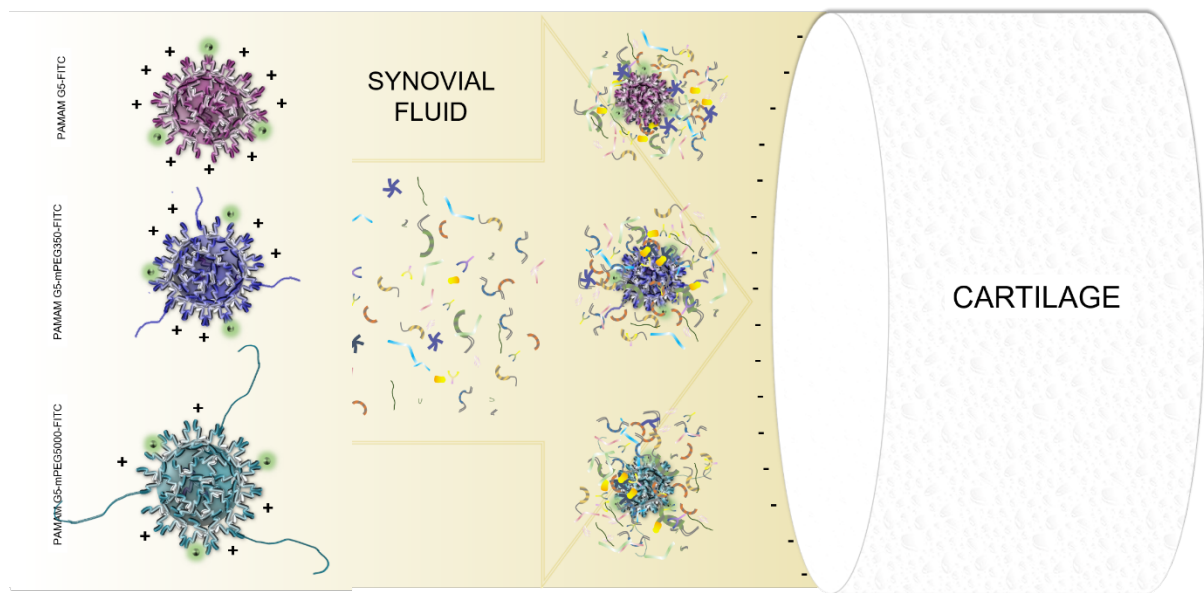
**Corresponding author: Alexandra Stubelius, Alexandra.stubelius@chalmers.se*

Postal address: Kemivägen 10, 41296 Gothenburg, Sweden

*Keywords: Drug delivery; cartilage, synovial fluid, PAMAM, osteoarthritis, rheumatoid arthritis,
protein corona / adsorption*

ABSTRACT

A major obstacle for joint drug delivery is the penetration of a dense, negatively charged cartilage matrix. By adapting their size, charge, and surface chemistry to the tissue's native environment, nanoparticles (NP) can improve the transport and efficacy of novel and conventional drugs. Although previous studies have extensively considered the aspects of cartilage tissue uptake, they have neglected to address the potential interactions between the particles and the components of the synovial cavity. By varying the lengths of methoxy polyethylene glycol (mPEG) and consequently the surface chemistry of the nanoparticles, we synthesized a fluorescently labeled, dendrimeric polyamidoamine (PAMAM)-based NP panel that was subjected to three different protein conditions including synovial fluid from RA or OA patients, as well as the conventional fetal calf serum (FCS). The effects of formed protein corona on the nanoparticles were evaluated in the cartilage and cellular uptake studies. Compared to non-protein covered NP, we observed a prominent impact of the origin of the protein coronas on the NP uptake into the cartilage, where the FCS derived coronas were taken up easier than the synovial fluid-derived coronas. Furthermore, we identified a candidate nanocarrier, NP₅₀₀₀, to be the most suitable for drug carrier applications in OA. Utilizing a quantitative proteomics approach, we identified similar profiles for RA and OA synovial fluid-derived protein coronas despite the distinction between the diseases. Proteins such as albumin, fibronectin, fibrinogen, various apolipoproteins, and others were present in high abundance on all panel members irrespective of the nanoparticle modifications. Nonetheless, nanoparticle and protein condition-specific differences were also observed between the groups. Our study, therefore, suggests that the biological protein abundance in the synovial fluid dictates the nanoparticle efficacy and uptake into the tissue, emphasizing the importance of biological milieu considerations for the joint drug delivery design and its translation into the clinics.



Abstract Figure

1. INTRODUCTION

A major obstacle for therapies targeting joint diseases has been to reach the chondrocyte cells deeply embedded in the extracellular cartilage matrix (ECM). This dense, avascular, and aneural network of large and highly negatively charged macromolecules pose a physical barrier to reach the cells, making retention time in the synovial space crucial to increase the likelihood of a therapeutic to be readily absorbed into the tissues and not being rapidly cleared^{1,2}. The challenge therefore lies in designing drug delivery strategies that penetrate the ECM tissue, enhance chondrocyte uptake, as well as avoid rapid immune clearance. Recent advancements in intra-articular drug delivery have leveraged both small sizes and electrostatic interactions with the anionic ECM^{1,3}, and the quest to solving these issues has received much attention for joint diseases in general, and for osteoarthritis (OA) in particular. Diseases such as OA are on the rise due to our increasingly aging and overweight population, yet there are no disease-modifying therapies available to slow down the disease progression. The World Health Organization (WHO) estimates that 9.6% of men and 18% of women aged 60 and above have symptomatic OA, and the increasing OA prevalence is predicted to majorly affect our societies². Simultaneously, rheumatoid arthritis (RA) has seen a revolution in treatment progress over the last

decades due to highly efficient biologics that reduce the autoimmune reaction degrading the cartilage⁴. Rheumatologists are now turning towards personalized medicine and biomarkers to improve treatment strategies further, potentially targeting cartilage structures in parallel with OA strategies. For both RA and OA, increasing the retention time of drug delivery vehicles in the synovial space would enhance therapeutic success as the fast turnover rate of the synovial fluid poses a great challenge for therapeutic strategies. Yet so far, no studies have addressed the potential effect of the synovial fluid composition on such drug delivery vehicles, which is vital to understand and predict pharmacokinetic profiles and behaviors. For systemic administration, it is well known that micro and nanoscale drug delivery approaches are immediately subjected to the high abundance of host-derived biological components such as proteins, carbohydrates, and lipids⁵. These bioactive components can alter the size and surface composition of the particles and equip them with a distinct biological identity, in turn, dictating their physiological and therapeutic outcomes⁵⁻⁷. Factors that have been proven to highly affect this biomolecular corona include size and charge, which are the main components leveraged for passive intra-articular drug delivery into the cartilage³. For systemic administration, it was shown that just a simple change from blood plasma to serum had a profound difference in both protein corona composition and nanoparticle fate, demonstrating the importance of selecting the appropriate environment to account for in vivo settings⁹. The aim of this study was therefore to examine the influence of protein coronas on small, cationic nanoparticles (NP) derived from OA synovial fluid compared to RA synovial fluid, as well as the more frequently used fetal calf serum (FCS) in order to understand the impact of formed coronas on nanoparticle efficacy and fate.

2. RESULTS AND DISCUSSION

2.1 MATERIAL COMPOSITION AND CHARACTERIZATION

In this study, we designed three drug-delivery vehicles based on polyamidoamine (PAMAM) generation 5 dendrimeric nanoparticles. They can be easily manipulated and tuned for charge and size by facile surface conjugation. Multiple surface amino groups give rise to the intrinsic positive charge of the nanoparticles. The cationic nature of these nanoparticles has paved the way for their use in drug delivery due to their electrostatic attraction to negatively charged materials such as nucleic acids and

extracellular matrix proteins¹⁰. However, since strong electrostatic interactions are not always desirable due to increased cytotoxicity, protein adsorption or decreased stability of the system, utilization of various polymers has been successfully explored for tuning the physicochemical properties and the surface chemistry of the particles^{11,12}. In particular, PEGylation has been an attractive strategy as PEG offers good stability, hydrophilicity, and biocompatibility. Additionally, the biological interactions of PEGs have been extensively studied in the context of immune system as they provide the so called “stealth effect” to avoid immune system clearance¹². Here, both the degree of PEGylation and the length of the polymer has proven to dictate the NP’s biological fate^{13,14}. We therefore designed three types of PAMAM-based particles that vary in PEGylation, providing distinct characteristics based on charge and surface chemistry. Two different mPEGs of varying molecular weights (350 or 5000) denoted as NP₃₅₀ and NP₅₀₀₀ were chosen to provide discrete hydrodynamic radii yet maintain the optimal <10 nm size suggested to be imperative for ECM penetration¹⁵. The third type of NP contained no PEG, denoted as NP₀ and serve as a control. PEGylation was performed according to Ma et al.¹⁶, and analyzed by ¹H-NMR (Supplementary Figure S1). To retain the positive PAMAM profile, PEGylations were performed using 2% surface conjugation. The size measurements were elucidated by dynamic light scattering for the relevant aqueous environment characterization followed by confirmation using transmission electron microscopy (TEM; Figure 1A and B). TEM micrographs in Figure 1A confirmed the dispersed nanoparticles at the expected sizes (theoretical size PAMAM G5= 5.4nm). The PAMAM nanoparticle solution pH was adjusted to 6 to protonate the tertiary PAMAM groups and to reduce the aggregation of the sample due to water evaporation. The hydrodynamic sizes of the NPs are shown in the Figure 1B. NP₀ nanoparticles measured 7.2 nm ± 2.8 nm, with a slight increase in size for NP₃₅₀ modification, 7.8 nm ± 2.5 nm, and the largest size as expected for NP₅₀₀₀ modification, 11.0 nm ± 4.4 nm. Similarities between NP₀ and NP₃₅₀ were also seen in zeta potential measurements where recorded values were +17.0 mV ± 1.78 mV and +16.0 mV ± 1.95 mV respectively, while NP₅₀₀₀ exhibited a lower value of +4.0 mV ± 2.57 mV. The changes in size and charge confirmed successful PEGylation modifications.

For tracking, the NPs were fluorescently labelled using fluorescein isothiocyanate, FITC, and the fluorescence signal of the NP panel was quantified using a fluorescence spectrophotometer. 30uM

nanoparticle suspensions showed a similar fluorescence intensity for all three NPs, indicating no quenching arising from intermolecular interactions in any of these systems (Figure 1D). At 526nm, the fluorescence intensities for NP₀ and NP₃₅₀ were 958 a.u. and 964 a.u. respectively, while NP₅₀₀₀ exhibited a peak of 924.5 a.u. at 527 nm.

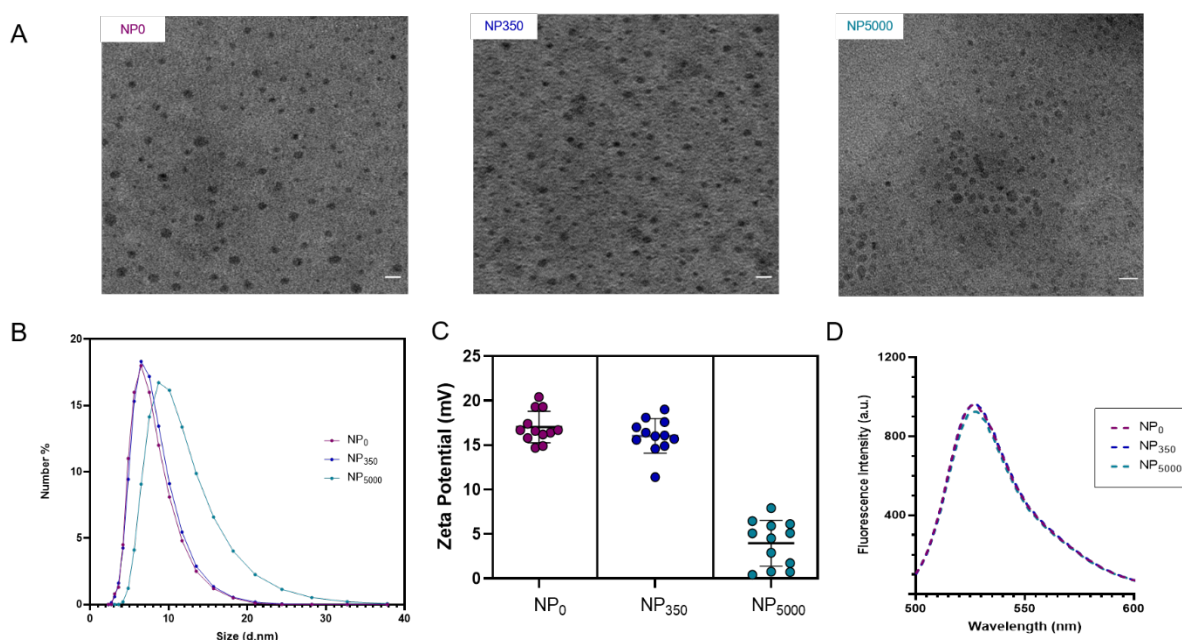


Figure 1. PAMAM-mPEG_x-FITC NP characterization. The sizes of the NPs were assessed with TEM (A) in a 15uM PBS suspension at pH=6. The hydrodynamic diameter of the particles was measured in 30uM, neutral pH environment and the values were extracted based on the size distribution by volume (B), and zeta potential was quantified using DLS (C). Green fluorescence FITC signal was measured and quantified $\lambda = \text{ex. } 483\text{-}14 \text{ nm}$, $\lambda = \text{em. } 530\text{-}30 \text{ nm}$ by a fluorescence spectrophotometer (D).

PAMAM dendrimer toxicity has been extensively investigated as their highly cationic charge has been associated with disruption of the negatively charged cellular membranes^{17,18}. In our study, we assessed the cytotoxicity of the nanoparticles on 3 different cell types including mouse fibroblast (L929), human chondrocyte (Tc28a2), and monocyte (U937) cell lines ranging from 100 uM to 12.5 uM to determine the optimal dose for biological studies. Resazurin metabolic activity assay revealed that all cell lines responded well to concentrations of equal to or below 50uM, while all concentrations of NP₅₀₀₀ was above 70% viability threshold for all three cell types (Supplementary Figure S2)¹⁵. This further

confirmed the successful PEGylation of our nanoparticles and suggested that these NPs can be used at relatively high concentrations in biological studies.

2.2 CARTILAGE UPTAKE STUDIES OF PROTEIN CORONA COATED NPs

Given that the nature of cartilage tissue is characterized by the negative charge due to the presence of carboxyl and sulfate groups on glycosaminoglycans present in the protein matrix, we wanted to investigate how the differences in our NP composition would affect the cartilage uptake. Porcine-derived explants are considered as optimal tissues to investigate cartilage-targeting drug delivery vehicles due to their biocompatibility similar thickness to humans^{19,20}. As our particles were labeled with FITC, we were able to track the reduced NP FITC signal in the wells after 4 or 24 hour-incubations. A reduced signal indicated tissue uptake and was quantified with an internal control by comparing T_{4h} and T_{24h} to the fluorescence signal at T_{0h} . In our initial trial, the NPs were added to the wells containing explants and supernatants, and their fluorescence was monitored over time. This study confirmed that despite the differences in size and charge, all three types of NPs were taken up into the tissues within 4 hours (Figure 2A). The further reduction in the signal observed after 24 hours indicates that all our designed sizes and charges represent viable cartilage penetrating NPs as this indicates increased cartilage uptake over time. As expected, the NP₅₀₀₀ displayed a larger variance in their signal over time, which we attribute to the free movement of mPEG chains in the aqueous environment, alluding to a dynamic surface chemistry of and a potential physical hindrance to ECM penetration.

The effect of protein adsorption on NPs and their influence on uptake efficacy are rarely addressed in NP characterization studies. Therefore, we assessed the cartilage uptake of NPs incubated with protein-rich synovial fluids from RA and OA patients. In comparison, we used the common protein and nutrient supplement FCS that is commonly utilized for in vitro therapeutic evaluation studies (Figure 2). Protein coronas were formed by exposing the NPs to either the synovial fluid or FCS for one hour and isolated by extensive washing to remove unbound proteins, leaving the hard protein corona adhered to the particles. To detect the differences in protein adherence due to fluid composition on a macro level, we first quantified the adhered protein content using the BCA quantification method (Figure 2B).

Interestingly, the surface chemistries of the particles did not change the number of adhered proteins, as we detected similar quantities per biological fluid on all three NP profiles. We found the most adhered proteins in the RA synovial fluid group, followed by FCS and OA. These differences may suggest a difference in the overall biological composition of the fluids, either on the level of overall protein abundance, or differences in the specific proteins present in the fluid.

Subsequently, we investigated if these differences in adhered proteins affected cartilage uptake. As the results from the protein-free NPs indicated no differences in cartilage uptake, any subsequent change would derive from interactions with the biological fluids and their composition. After 4 and 24h incubation with cartilage explants, we noted no difference in fluorescence for the NP₀ nor NP₃₅₀ with hard coronas from the synovial fluid samples (Figure 2C and D), suggesting a major uptake interference caused by the synovial fluid-derived protein coronas. In contrast, we detected a significant decrease in fluorescence for both NP₀ and NP₃₅₀ particles with protein coronas derived from FCS. This difference was found despite a reduced amount of adhered proteins from the OA fluid compared to FCS, and the increased amount of adhered proteins on the particles from the RA fluid. Taken together, this indicates that the protein identity has a larger influence on cartilage uptake than the overall amount of adhered proteins, which has major implications for translational studies with NP-based drug delivery vehicles. Interestingly, the NP₅₀₀₀ designed with a reduced positive charge but to be more biocompatible displayed a significant decrease in fluorescence for all NP₅₀₀₀ coronas, suggesting that a design with longer PEG-chains attracts a favorable corona identity for cartilage uptake, and suggests a design representing a promising drug delivery vehicle for targeting arthritis.

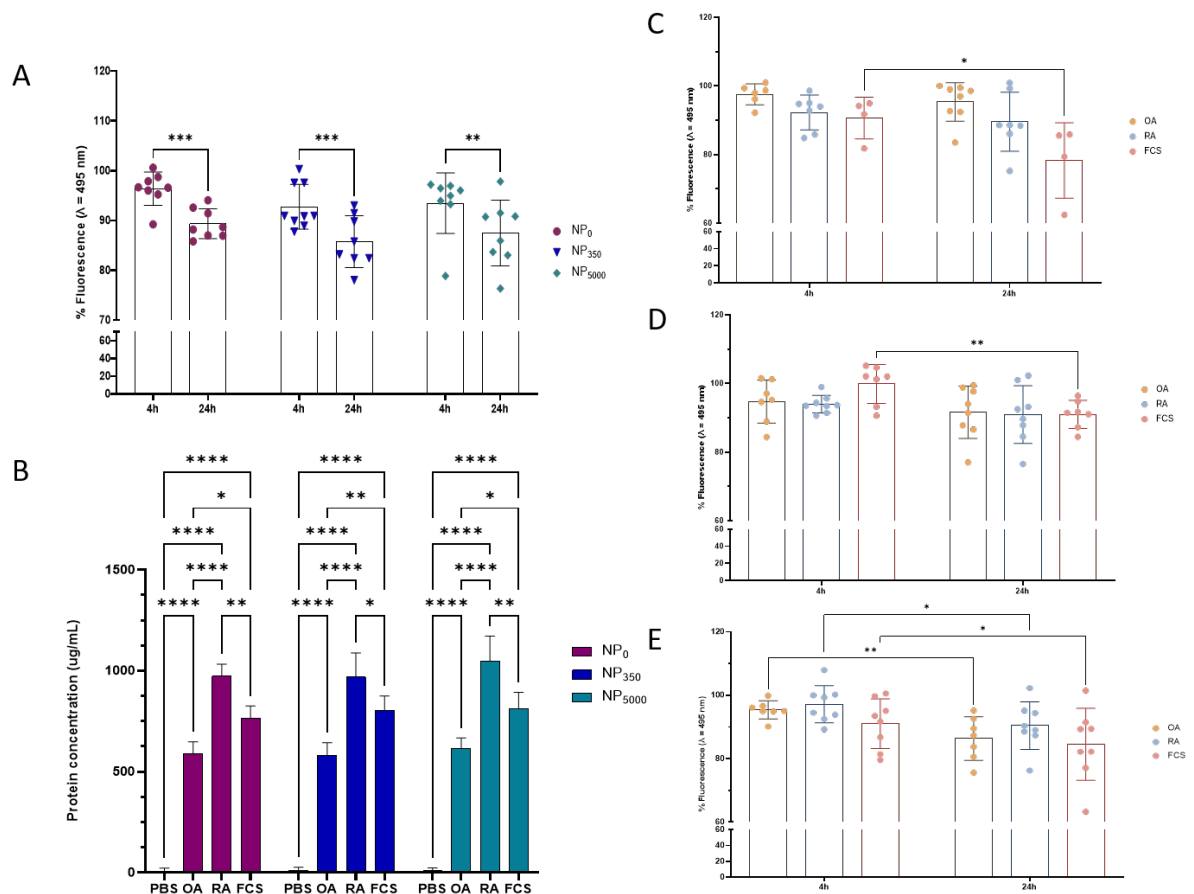


Figure 2. Investigation of PAMAM-mPEG_x-FITC nanoparticle uptake to the cartilage tissue explants. 30μM of NPs were administered to cartilage explants and incubated for 4h or 24h. FITC signal was normalized to T0 after T4 or T24 hours and detected using a fluorescence spectrophotometer and nanoparticle uptake into the cartilage tissue was assessed under regular laboratory conditions using PBS buffer as the solvent (A). Each NP suspension was subjected to three different protein abundant conditions – OA = pooled OA patient synovial fluid (2f/2m); RA = pooled RA patient synovial fluid (4f/1m); FCS = fetal calf serum. The adhered protein content was assessed using the BCA assay (B). The influence of the formed protein corona on cartilage uptake was compared for the NP₀ (C), the NP₃₅₀ (D), and the NP₅₀₀₀ (E). The data is representative of 3 independent experiment repeats, n= 4-9. Error bars represent standard deviations, while significance tests were performed using a 2-way ANOVA with Tukey's multiple comparisons test, where $p \leq 0.05$ (*), $p \leq 0.01$ (**), $p \leq 0.001$ (***), $p \leq 0.0001$ (****).

2.3 PARTICLE UPTAKE BY CHONDROCYTES AND MONOCYTES

For treatments aiming to target joints, it is important not only to consider the tissues but also the cellular uptake. In OA in particular, it is important to assess the capacity of drug delivery vehicles to enter chondrocytes as many drugs aim to alter the function of these ECM-producing cells. Simultaneously, it is important to avoid phagocytic clearance by the immune cells as this could lead to elimination from the synovial space, cytotoxicity, and result in unsuccessful therapeutic effects. The phagocytic clearance of particles is even more relevant in the inflammatory phase, especially for autoimmune diseases such as RA which has an overactivated immune system. Here, cellular uptake of NPs is highly influenced by the protein corona, especially in their interactions with the immune system²¹. Therefore, we evaluated the cellular uptake of our protein-covered NPs in both human chondrocyte and monocyte cell lines. Cellular association studies based on flow cytometry demonstrated that the formed protein corona indeed affected the uptake in the different cells (Figure 3) when followed over time. NPs exposed to FCS proteins were uptaken to a greater extent than the NPs exposed to synovial fluids (Figure 3A, B, D, E), in line with the uptake into cartilage. Interestingly, the NP₅₀₀₀ displayed less uptake by chondrocytes with a maximum of 60%, compared to NP₀ or NP₃₅₀ that reached 80% uptake after 10 hours (Figure 3A, B, C). Nonetheless, NP₅₀₀₀ covered with proteins from OA synovial fluid exhibited the highest uptake in chondrocytes. For monocytes, cellular uptake again favored the FCS condition, whereas synovial fluid-coated particles were not taken up to the same extent (Figure 3D, E, F). Similar trends were noted among NP₀ and NP₃₅₀, however, unexpectedly low levels were recorded for the NP₅₀₀₀ particles. As increased PEGylation results in stealth properties and avoidance of monocyte clearance, this data suggest that the NP₅₀₀₀ manages to avoid cellular uptake, in line with previous studies on PEGylation²². However, we cannot exclude the possibility that these particles may be taken up earlier than within 30min. As avoiding uptake and clearance by monocytes are desirable properties for NPs, the NP₅₀₀₀ would continue to hold promise as a nanocarrier design for OA applications.

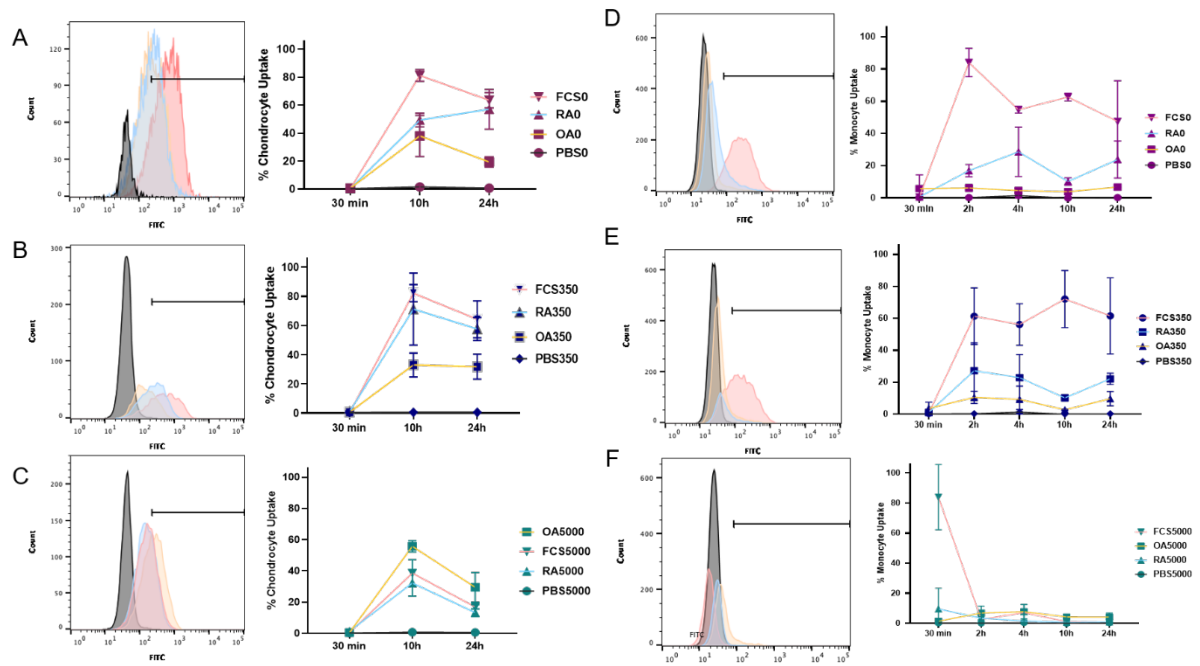


Figure 3. Assessment of PAMAM-mPEGx-FITC nanoparticle uptake in chondrocytes (A, B, C) and monocytes (D,E,F) after the indicated timepoints. NPs were preincubated with either PBS or OA, RA, or FCS for 1 hour before washing. % uptake refers to the proportion of cells with positive fluorescence above background control, stemming from FITC-labelled NPs analyzed by flow cytometry. Flow cytometry histograms represent association with NP₀ (A,D), NP₃₅₀ (B,E) or NP₅₀₀₀ (C,F). Data are shown as the mean and SD of, n=3-4, 1-3 independent experiments.

2.4 CHARACTERIZATION OF PROTEIN CORONA-COATED NPS

As NP surface chemistry modifications and protein conditions influenced both tissue and cellular uptake, we submitted the NPs for a global proteomic analysis to identify key differences between the NP composition and biological relevance of the adhered proteins. Using label free quantification, each NP was analyzed using LC-MS/MS. Obtained fragment masses and peptide sequences were matched with the organism specific UniProt (Swiss-Prot) sequence peptidomes. Based on previous proteome studies in late stage OA synovial fluid, we anticipated to detect an abundance of proteins associated with joint damage such as ECM proteins, proteins involved in complement cascade, coagulation, and an acute immune response²³. The OA synovial fluid profile was also expected to, and indeed was confirmed to, resemble the profile of the RA synovial fluid, reaching a stage of chronic inflammation,

joint damage, and abnormal bone changes. For RA, synovial fluid has been reported to contain a large proteome (>950 proteins) of various extracellular and cytoplasmic proteins from multiple pathways, including those playing a role in nucleic acid metabolism, hyaluronan regulation as well as highly abundant immune response proteins²⁴. The most abundant proteins identified in our synovial fluid samples included albumin (ALB), proteoglycan 4 / lubricin (PRG4), fibronectin (FN1), inflammation associated proteins, and numerous apolipoproteins. Such composition indicates the derivation of the synovial fluid from blood plasma. The high abundance of components such as myeloperoxidase (MPO), complement proteins such as C1s, C3, C4a/b, C9, hemoglobin subunit beta (HBB) confirmed the inflammatory state, as well as the findings of immunoglobulins (IGHM, IGHG1, IGHA1, JCHAIN). ECM associated proteins included inter-alpha-trypsin inhibitor heavy chains (ITIH1, ITIH2, ITIH4), Cartilage acidic protein 1 (CRTAC1), Cartilage oligomeric matrix protein (COMP); Alpha-2-HS-glycoprotein (AHSG) – which are associated with cartilage remodeling and the mineralization process, confirming the late stage of the disease and abnormal bone changes. In addition, we found proteins such as coagulation factor heparin cofactor 2 (SERPIND1) and prothrombin (F2); actin-binding gelsolin (GSN); histone components (H4C1, H3C1, H2AZ), which all take part various cell processes and protein transport, indicating a highly active biological environment.

However, despite the species difference, the most abundant proteins found in the FCS conditions correlated with the majority of the proteins found in the synovial patient samples. Similarities between the synovial fluid and FCS included albumin, complement factors, fibrinogen, inter-alpha-trypsin inhibitor heavy chains (ITIH family), and various apolipoproteins. Also here, we found ECM-associated proteins such as aggrecan (ACAN), lumican (LUM) and thrombospondin-1 (THBS1), as well as cytoskeletal organization dictating proteins such as actin (ACTB) and a number of keratins (KRT10, KRT5, KRT79). These similarities indicate that the biological fluid composition is similar between plasma, serum, and synovial fluid, and that the differences we detected in particle uptake - either the tissues or the cells- depend on the NP interactions with particular proteins.

In total, we identified 52, 58, and 59 statistically significant differentially expressed proteins among the NPs for OA, RA, and FCS conditions, respectively. To create a general overview between protein conditions, we grouped the proteins according to their molecular function and protein classification

using Gene Ontology (GO) based PANTHER classification system and database. The obtained results in Figure 4 illustrate that a large part of the proteins adhered to the PAMAM-mPEG_x-FITC NPs found in all three protein conditions exhibited binding or catalytic activity functions (Figure 4A, B, C), and we observed functional similarities between the different protein environments despite FCS proteins arising from a different animal species.

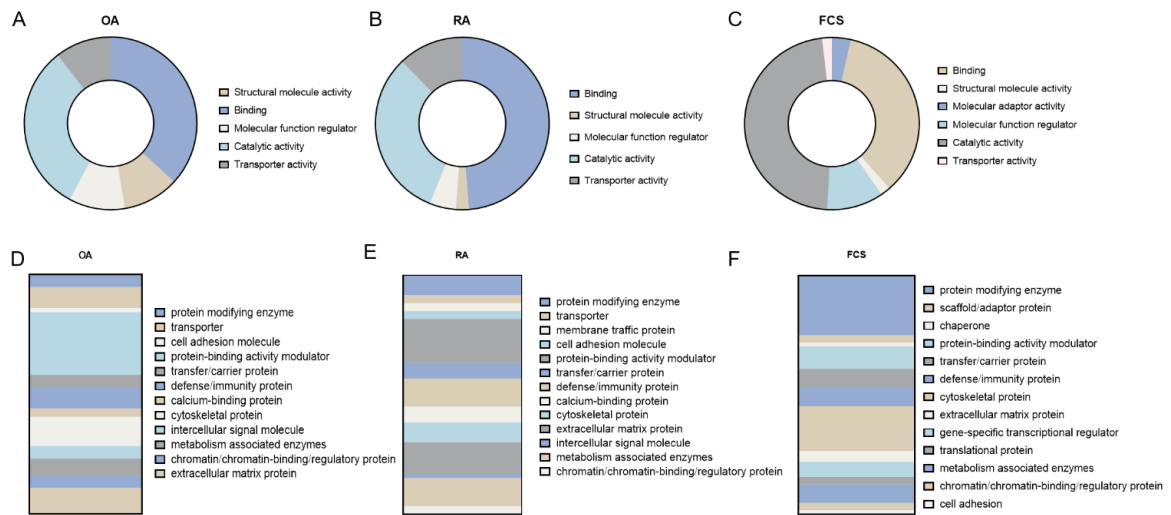


Figure 4. Pathway enrichment analysis for the differential protein abundances on the coronas detected in the panel of PAMAM-mPEG_x-FITC NPs. PANTHER based analysis revealed molecular function of the identified proteins in human patient OA synovial fluid (A), human patient RA synovial fluid (B), and bovine fetal calf serum (FCS) (C) samples. To further compare the difference between the detected proteins on the NP coronas, protein classification was also elucidated for the OA (D), RA (E), and FCS (F) samples using the same analysis comparison.

Protein classification analysis revealed that in the synovial fluid samples, protein activity binding modulators such as C3, C4BPA, C5, ITIH1, ITIH2, ITIH4, SERPINA3, ARF4, HRG, GFA, HSPB1, and others composed the largest part of differentially abundant proteins (Figure 4D and E) comprising of 26% and 18% of the total significant protein count in OA and RA, respectively. In contrast, the largest group of proteins in the FCS samples were classified as protein modifying enzymes and included 25% of the significant proteins, followed by cytoskeletal proteins which comprised 17% of the total significant protein count.

In depth analysis of the identified significant differential proteins among the NPs for OA, RA, and FCS conditions is depicted in the Figure 5. Common proteins between OA and RA included COMP, ITIH1, ITIH2, and SIGLEC5. Interestingly, these proteins were upregulated in the NP₃₅₀ particle, while they were mainly downregulated in NP₅₀₀₀. For OA, the NP₀ showed a similar profile to NP₅₀₀₀ with upregulated abundances seen in the proteins involved in the protein transport such as ARF4, ACAP1, RP2 (Figure 5A). As these NPs displayed remarkable differences in chondrocytes uptake, we concluded that while interesting, these proteins do not dictate NP uptake. Instead, TOM1 represents an interesting candidate that could direct NP chondrocyte uptake, as this protein was found mostly abundant on the NP₅₀₀₀ and is responsible for recruiting clathrin and driving endosomal cellular uptake²⁵.

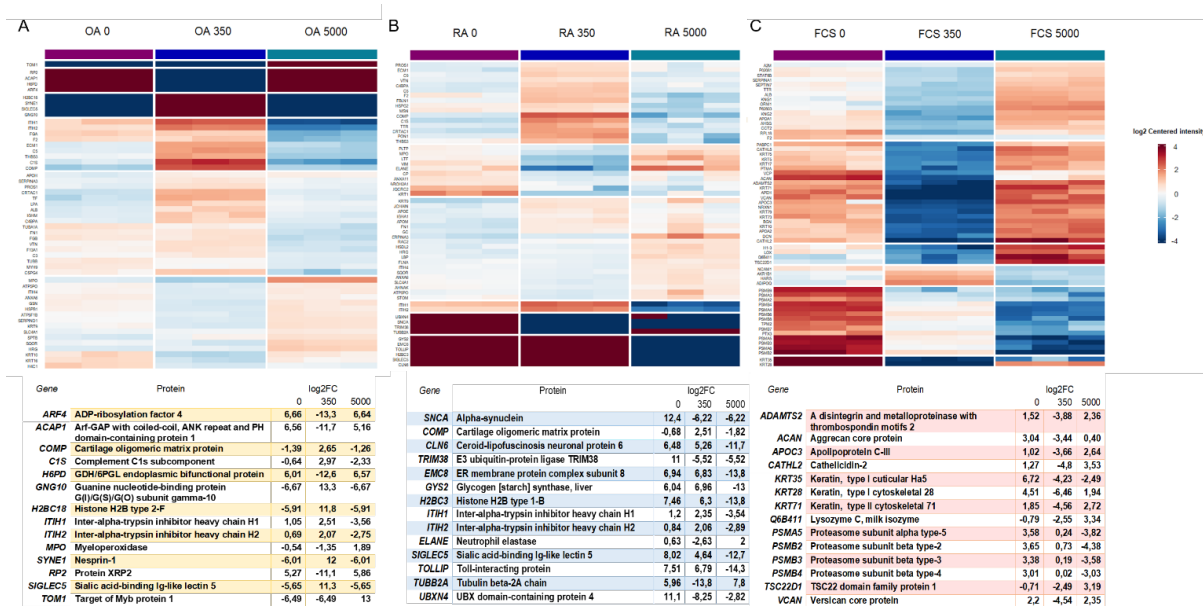


Figure 5. Heat maps of the differentially expressed significant proteins associated with individual protein coronas on NP₀, NP₃₅₀, and NP₅₀₀₀ exposed to late-stage OA synovial fluid (52) (A), RA synovial fluid (58) (B), or commercially available FCS (59) (C). The red and blue color scheme indicates high and low abundance of LFQ intensities represented as log₂FC. The tables below summarize the top 14 differentially expressed proteins among the NP groups.

For RA, we noticed the highest chondrocyte uptake with the NP₃₅₀ after 10 hours, reaching 70%, and was abundant in EMC8, GYS2, H2BC3, TOLLIP (Figure 5 B). Interestingly, TOLLIP has been

reported to associate with the previously mentioned TOM1 protein. Together, they would promote recruitment of clathrin onto the endosomes, alluding to the potential endocytic pathways that drive NP uptake in the cells²⁵. The other abundant proteins, however, have yet to be determined to play a role in NP cellular uptake and cannot explain the increased signal detected in the chondrocyte studies.

With regards to chondrocyte uptake for NP coronas derived from FCS, both NP₀ and NP₃₅₀ reached almost 80% at 10 hours. NPs with proteins from FCS showed distinct differential abundances for a variety of proteasome subunits (Figure 5 C), in particular with multiple members of PSMB and PSMA families. The FCS₅₀₀₀ profile was distinct as it lacked the abundance of the proteasome subunits, and also showed the lowest cellular uptake, indicating that a protein corona with a high abundance in proteasomes have a higher probability for cellular uptake by both chondrocytes and monocytes, which could have implications for drug delivery vehicles.

In general, the proteome analysis detected multiple proteins associated the NPs. The fact that the FCS and synovial fluids display such large discrepancy both in particle uptake as well as proteome profiles indicate how important these profiling studies are in order to fully understand NP interactions with biological fluids and environments and how they affect the NP therapeutic potential.

Conclusion

The nature of the intrinsic biological environment is an important consideration that often is neglected in many drug delivery vehicle studies²⁶. To the best of our knowledge, the formation of rheumatic synovial fluid-derived protein coronas and the subsequent effects on the nanocarrier uptake have not been previously evaluated. Our study addressed this issue by evaluating three types of nanoparticles differentially PEGylated nanoparticles, NP₀, NP₃₅₀, NP₅₀₀₀, and the effects of their interactions with synovial fluids from patients with RA and OA, and commonly used fetal calf serum, FCS on cartilage tissue and cellular uptake. The lack of significant differences in the cartilage uptake of protein-free nanoparticles revealed that the nanoparticle uptake into the cartilage was mainly driven by the differences between the formed protein coronas. We detected a decrease in the cartilage uptake for the samples exposed to the patient-derived synovial fluids, while FCS-derived protein coronas appeared to promote NP uptake. Interestingly, NP₅₀₀₀ proved to also be significantly uptaken into the cartilage after

being subject to OA synovial fluid-derived proteins, suggesting its relevance for OA drug delivery strategies. A similar trend was seen in the cellular uptake studies, where we examined NP uptake in chondrocyte and monocyte cell lines. FCS-derived coronas offered the highest degree of cellular uptake, except for NP₅₀₀₀ which exhibited a highest degree of uptake under the OA conditions in chondrocytes. Surprisingly, we noted a low uptake of NP₅₀₀₀ into monocytes, suggesting that the effect of PEGylation may spare the NP uptake into phagocytic cells without compromising the uptake into the cartilage cells. We also determined the significant protein differences between the nanoparticles and the corresponding protein conditions revealing the significance of the protein environment. Differential adherence of proteins such as Target of Myb protein 1, TOM1 and toll interacting protein, TOLLIP, also known to be involved in clathrin mediated endocytosis might explain the differences seen in cartilage and cell uptake studies. Additionally, we were also able to demonstrate the specificity of certain proteins such as COMP and ITIH1/2 to NP₃₅₀ in both RA and OA conditions, suggesting that the surface chemistry of the NP plays a key role in protein corona composition. Our study is in line with the previous research emphasizing the effect of biologically rich environments such as serum and plasma and their effect on establishing the biological NP identity and its impact for the therapeutic translation.

REFERENCES

1. Bajpayee, A. G. & Grodzinsky, A. J. Cartilage-targeting drug delivery: Can electrostatic interactions help? *Nat. Rev. Rheumatol.* **13**, 183–193 (2017).
2. Glyn-Jones, S. *et al.* Osteoarthritis. *Lancet* **386**, 376–387 (2015).
3. Bajpayee, A. G., Scheu, M., Grodzinsky, A. J. & Porter, R. M. Electrostatic interactions enable rapid penetration, enhanced uptake and retention of intra-articular injected avidin in rat knee joints. *J. Orthop. Res.* **32**, 1044–1051 (2014).
4. Pitzalis, C., Choy, E. H. S. & Buch, M. H. Transforming clinical trials in rheumatology: towards patient-centric precision medicine. *Nat. Rev. Rheumatol.* **16**, 590–599 (2020).
5. Lundqvist, M. & Cedervall, T. Three Decades of Research about the Corona Around Nanoparticles: Lessons Learned and Where to Go Now. *Small* **16**, 2000892 (2020).
6. Monopoli, M. P., Åberg, C., Salvati, A. & Dawson, K. A. Biomolecular coronas provide the biological identity of nanosized materials. *Nat. Nanotechnol.* **7**, 779–786 (2012).
7. Madathiparambil Visalakshan, R. *et al.* The Influence of Nanoparticle Shape on Protein Corona Formation. *Small* **16**, 2000285 (2020).
8. Walkey, C. D. & Chan, W. C. W. Understanding and controlling the interaction of nanomaterials

- with proteins in a physiological environment. *Chem. Soc. Rev.* **41**, 2780–2799 (2012).
9. Mirshafiee, V., Kim, R., Mahmoudi, M. & Kraft, M. L. The importance of selecting a proper biological milieu for protein corona analysis in vitro: Human plasma versus human serum. *Int. J. Biochem. Cell Biol.* **75**, 188–195 (2016).
 10. Abedi-Gaballu, F. *et al.* PAMAM dendrimers as efficient drug and gene delivery nanosystems for cancer therapy. *Applied Materials Today* vol. 12 177–190 (2018).
 11. Kim, Y., Klutz, A. M. & Jacobson, K. A. Systematic investigation of polyamidoamine dendrimers surface-modified with poly(ethylene glycol) for drug delivery applications: Synthesis, characterization, and evaluation of cytotoxicity. *Bioconjug. Chem.* **19**, 1660–1672 (2008).
 12. Rosenblum, D., Joshi, N., Tao, W., Karp, J. M. & Peer, D. Progress and challenges towards targeted delivery of cancer therapeutics. *Nature Communications* vol. 9 1–12 (2018).
 13. Schöttler, S. *et al.* Protein adsorption is required for stealth effect of poly(ethylene glycol)- and poly(phosphoester)-coated nanocarriers. *Nat. Nanotechnol.* **11**, 372–377 (2016).
 14. Milton Harris, J. & Chess, R. B. Effect of pegylation on pharmaceuticals. *Nature Reviews Drug Discovery* vol. 2 214–221 (2003).
 15. Bajpayee, A. G., Wong, C. R., Bawendi, M. G., Frank, E. H. & Grodzinsky, A. J. Avidin as a model for charge driven transport into cartilage and drug delivery for treating early stage post-traumatic osteoarthritis. *Biomaterials* **35**, 538–549 (2014).
 16. Ma, P. *et al.* Targeted delivery of polyamidoamine-paclitaxel conjugate functionalized with anti-human epidermal growth factor receptor 2 trastuzumab. *Int. J. Nanomedicine* **10**, 2173–2190 (2015).
 17. Janaszewska, A., Lazniewska, J., Trzepiński, P., Marcinkowska, M. & Klajnert-Maculewicz, B. Cytotoxicity of dendrimers. *Biomolecules* vol. 9 330 (2019).
 18. Albertazzi, L. *et al.* In vivo distribution and toxicity of PAMAM dendrimers in the central nervous system depend on their surface chemistry. *Mol. Pharm.* **10**, 249–260 (2013).
 19. Macfadyen, M. A. *et al.* The commercial pig as a model of spontaneously-occurring osteoarthritis. *BMC Musculoskelet. Disord.* **20**, 1–12 (2019).
 20. Cone, S. G., Warren, P. B. & Fisher, M. B. Biomechanical considerations of animal models used in tissue engineering of bone. *Tissue Eng. - Part C Methods* **23**, 763–780 (2017).
 21. Ju, Y. *et al.* Person-specific biomolecular coronas modulate nanoparticle interactions with immune cells in human blood. *ACS Nano* **14**, 15723–15737 (2020).
 22. Sivaram, A. J. *et al.* Controlling the biological fate of micellar nanoparticles: Balancing stealth and targeting. *ACS Nano* **14**, 13739–13753 (2020).
 23. Ritter, S. Y. *et al.* Proteomic analysis of synovial fluid from the osteoarthritic knee: Comparison with transcriptome analyses of joint tissues. *Arthritis Rheum.* **65**, 981–992 (2013).
 24. Bhattacharjee, M. *et al.* Synovial fluid proteome in rheumatoid arthritis. *Clin. Proteomics* **13**, (2016).
 25. Katoh, Y., Imakagura, H., Futatsumori, M. & Nakayama, K. Recruitment of clathrin onto endosomes by the Tom1-Tollip complex. *Biochem. Biophys. Res. Commun.* **341**, 143–149 (2006).

26. Berrecoso, G., Crecente-Campo, J. & Alonso, M. J. Unveiling the pitfalls of the protein corona of polymeric drug nanocarriers. *Drug Deliv. Transl. Res.* **10**, 730–750 (2020).

3. Experimental Section

3.1 Materials and Reagents

Ethylenediamine core amino-terminated PAMAM dendrimer Generation 5 manufactured by Dendritech (CAS: 163442-68-0), methoxypolyethylene glycols (mPEG) 350 and 5000 (CAS:9004-74-4), 4-(Dimethylamino)pyridine (DMAP) $\geq 99\%$ (CAS:1122-58-3), PMA (CAS:16561-29-8), 4-nitrophenyl chloroformate (4-NPC) 97% (7693-46-1) manufactured by Acros Organics, fluorescein isothiocyanate isomer I (CAS:3326-32-7), resazurin sodium salt (CAS: 62758-13-8), and chondroitin 4-sulfate sodium salt from bovine trachea (39455-18-0) were all purchased from Sigma-Aldrich (Munich, Germany).

DPBS (1X) without calcium and magnesium (manufactured by Gibco), dichloromethane (CAS:75-09-2), dimethyl sulfoxide (CAS: 67-68-5), deuterium oxide (CAS:7789-20-0) manufactured by Acros Organics, DMEM (Dulbecco's Modified Eagle's Medium), RPMI 1640 (Roswell Park Memorial Institute), fetal bovine serum (FBS), GlutaMAX by Gibco, and Pierce BCA protein assay kit were all purchased from Fisher Scientific (Waltham, USA).

3.2 Material Synthesis

3.2.1 PAMAM PEGylation

First, mPEG 350 or 5000, 4-NPC, and DMAP were combined using a molar ratio of 1: 1.5: 1.1, respectively and dissolved using dropwise addition of DCM. The reaction was stirred for 24 hours under nitrogen flow at room temperature. To obtain the product, most of the solvent was removed using rotary evaporator, while the product was precipitated over the excess chilled diethyl ether, collected using vacuum filtration and dried. The product of activated mPEG was purified by recrystallization using chloroform and diethyl ether, 10:1.

PAMAM G5 solvent was switched from methanol to deionized water. 1.585mM of PAMAM solution was diluted 1:10 using NaHCO_3 and pH value was adjusted to 8.0 ± 0.08 . mPEG350 and mPEG5000 were solubilized in DMSO while in 0% PEG condition, no mPEG was added. PEGylation was executed combining these solutions in a stoichiometric ratio of 1:3 for PAMAM and (no) mPEG respectively. Mixtures were vortexed, covered and incubated overnight while shaking at room temperature. Samples were then dialyzed against deionized water using Spectra/Por 3 Regenerated Cellulose 6-8kD MWCO

tubing to remove DMSO and unreacted reagents. Synthesized compounds were lyophilized and stored in the fridge until further use.

3.2.1.1 Nuclear magnetic resonance (NMR)

¹H NMR spectra of the compounds were recorded with Agilent VnmrS spectrometer at 400 MHz. Samples were solubilized in D₂O unless otherwise stated. Data was analyzed using MestReNova version 14.1.1.

3.2.2 FITC conjugation

PEGylated PAMAM compounds (NP₀, NP₃₅₀, NP₅₀₀₀) were dissolved in PBS (pH=7.4) at 5mg/mL and were allowed to react with fluorescein isothiocyanate isomer I (FITC) which was dissolved in acetone at 1:5 molar ratio respectively. The reaction was carried on in the dark for 12h, stirring at room temperature. The samples were then dialyzed to remove unreacted FITC molecules, lyophilized and set at the concentration of 30μM in PBS (pH=7.4).

3.2.3 FITC conjugation quantification

FITC conjugation was confirmed using Varian Cary 50 Bio UV/Vis spectrophotometer. PBS served a baseline for the measurements. Fluorescence signal was quantified using a CLARIOstar Plus (BMG Labtech, Offenburg, Germany) microplate reader with settings for FITC (λ_{ex} 483-14 nm/ λ_{em} 530-30 nm). Briefly, each type of FITC-labelled nanoparticles was dissolved in methanol and diluted with PBS to the final concentration of 2 μg/ml. Standard curve was generated by preparing FITC standard solutions of 0.5 to 40ng/mL. Percent labelling efficiency was extracted as the proportion of FITC weight to the weight of PAMAM- (0%; 2%-350; 2%-5000) mPEG-FITC in the solution.

3.3 Transmission Electron Microscopy (TEM)

Nanoparticles were diluted to 15uM and the pH was adjusted to 6. Samples were briefly sonicated and a drop of dendrimeric nanoparticle suspension was placed on a 3mm holey carbon film coated copper grid (Ted Pella, Inc., Redding, California) and allowed to air-dry at room temperature. The samples were imaged using Orius CCD camera mounted on FEI Tecnai T20 transmission electron microscope.

3.4 Dynamic Light Scattering (DLS)

30uM nanoparticle suspensions in PBS were assessed using Zetasizer Nano ZS system (Malvern Instruments, UK). Size of the nanoparticles was measured using disposable semi-micro UV-cuvettes

(VWR, Leuven, Belgium), while for zeta potential measurements folded capillary zeta cells (DTS1070, Malvern, UK) were used. Hydrodynamic size and zeta potential is reported as a mean of three runs for each sample size (d.nm) \pm s.d (d.nm).

3.5 Protein corona isolation/formation

3.5.1 Patient-derived synovial fluid samples

All patients have provided informed consent and the procedure was approved by the Ethics Committee of Gothenburg University (Ethical approval Dnr: 573-07). Synovial fluid samples from 5 (4f/1m) RA patients and 4 (2f/2m) late OA patients were collected during aseptic aspiration of knee joints at the Rheumatology Clinic and at the Orthopaedic Clinic respectively, Sahlgrenska University Hospital, Gothenburg, Sweden.

3.5.2 Protein Corona Formation

5 RA, 4 OA patient synovial fluid and control FBS samples were pooled according to the disease profile (5×10^8 particles or 2 μ g), diluted 1:20 in PBS and mixed with 30 μ M solution of PAMAM- (0%; 2%-350; 2%-5000) mPEG-FITC (1:1, v/v). The samples were incubated at 37°C while shaking for 1h. The particles were subsequently spun down at 15,000 x g for 15 minutes, washed twice with chilled PBS. The particles with adhered protein corona were resuspended to the final volume of 2 ml to a 1 μ g/ml (2.5×10^8 particles/mL) concentration in PBS and further processed according to below studies.

3.6 Cellular interactions with nanoparticles

Cellular studies focused on utilizing Tc28a2 chondrocyte cell line (a kind gift from Dr. Cronstein's lab at NYU Langone, USA) and cultured in DMEM, supplemented with 10% FBS and 1% GlutaMAX and grown at 5% CO₂, relative humidity of 95%, and 37°C.

3.10 Protein quantification of NP coronas

Protein content in the supernatant of the explants was assessed using a Pierce BCA protein assay kit according to manufacturer's instructions. Briefly, 10 μ l of the explant study supernatants were mixed with working reagent for 30 seconds and incubated for 30min at 37°C. Plate was allowed to cool to room temperature and the absorbance values at were measured at the wavelength of 562 nm. Standard curve of bovine serum albumin ranged from 2000 μ g/ml to 25 μ g/ml. The experiments were performed independently 3 times in triplicates, n= 4-9.

3.7 Cellular nanoparticle-corona uptake

Cell medium was replaced to remove FBS as this could contribute to additional corona formation and thus was treated as one of the controls. The cells were seeded at 1×10^5 cells/well in a 48-well plate. The cells were incubated with the particles at the indicated timepoints, washed three times in FACS buffer (1% FBS, 0,1 % NaN₃ in 1xPBS) and flow cytometry analysis was performed using Guava EasyCyte 8HT (Millipore, Darmstadt, Germany). Live cells were analyzed (after FSC/SSC exclusion of dead cells, >5000 cells) from within the gate were counted. The FITC was excited by a 488 nm laser, and fluorescence was detected through a 525/30 nm filter. The mean cellular uptake of FITC-labeled NP was estimated as the average fluorescence intensity of all cells within the gate. The data was obtained in 1-3 independent experiments and is represented as the means with SD, n=3-4 with acquisition range of 5000-10000 cells. All flow cytometry data was analyzed and visualized using FlowJo software.

3.8 *Ex vivo* porcine-explant model of fluorescent nanoparticle uptake

Porcine tissue was obtained from the Experimental Biomedicine animal facilities under the 3R principle (Gothenburg, Sweden). The specimens entailed unexposed joints of the pig legs with femur and tibia still intact. Explants were frozen in PBS+PI+P/S (1%). When thawed or freshly introduced to culture, explants were allowed to equilibrate in the DMEM (without phenol red, supplemented with 25mM HEPES) overnight before the experiment. To quantify FITC-labelled nanoparticle uptake into the cartilage, 4 mm puncher (Kai Medical, Honolulu, USA) biopsies were used to produce uniform explants of porcine cartilage with similar thickness to human. Explants were weighed to ensure uniformity before the experiments were started. Prior to nanoparticle administration, explants were placed in culture with 150µl DMEM lacking phenyl red, supplemented with 1% 10,000 U/mL Penicillin, Streptomycin (Gibco) and protease inhibitors (Roche, Switzerland) and allowed to equilibrate overnight. 100µl of 30µM NP₀, NP₃₅₀, NP₅₀₀₀ protein corona nanoparticle solution was administered to the designated explants and incubated for 4 or 24 hours. The resultant FITC fluorescence in the supernatants and the explants was read at λ_{ex} 483-14 nm/ λ_{em} 530-30 nm using FITC settings on CLARIOstar Plus (BMG Labtech) as mentioned above. Each explant condition was performed in triplicates and repeated independently two-times. FITC amount was quantified using the FITC-based standard curve.

3.9 Statistics

Data is presented as mean values \pm SD unless otherwise indicated. Statistical analysis was performed using GraphPad Prism (GraphPad Software) version 9.0.2. Two-way analysis of variance (ANOVA) was used to compare independent groups based on particle and protein conditions; all groups were statistically compared followed by Tukey's post hoc multiple comparisons test. P values <0.05 were considered statistically significant.

3.9.1 Proteomic Analysis

Nanoparticles with isolated protein coronas were pelleted, snap frozen using liquid nitrogen and submitted to the Proteomics Core Facility (Gothenburg, Sweden). Briefly, proteins were digested into peptides using MS-grade trypsin and analyzed by nanoscale liquid chromatography-tandem mass spectrometry LC MS/MS. MS scans were performed in the Orbitrap. Precursor ions were isolated in the quadrupole with a 0.7 m/z isolation window, with dynamic exclusion set to 10 ppm and duration of 45 seconds. Produced MS2 fragment ions were detected in the ion trap. Mascot search engine was used to match the discovered peptide sequences against SwissProt human and bovine protein database using Proteome Discoverer. Data was analyzed using label free quantification (LFQ) method and the protein false discovery rate were set to 1%. Statistical and differential analysis along with the data representations were performed in R (R Foundation for Statistical Computing), using LIMMA, DEP, and ComplexHeatmap R packages. To account for inconsistencies and skewness in the obtained data, data was analyzed using the Mann Whitney Wilcoxon test followed by the Benjamini–Hochberg multiple hypothesis correction. Significance threshold was set for the adjusted p values of <0.05 and ratio change of >1.5 fold. Enrichment analysis to elucidate the molecular functions and classifications of the significant proteins was performed using Gene Ontology (GO) based PANTHER classification system. Synovial fluid samples were matched to human (*Homo sapiens*), while FCS samples were matched to the bovine (*Bos taurus*) databases.

2.5 AUTHOR CONTRIBUTIONS

UvM and A.S designed the studies. UvM synthesized the polymers, conducted the in vitro and ex vivo studies and performed analysis. G.E conducted the NMR studies and analysis. T.S and L.R performed in vitro assays and analysis. A.K.H.E provided patient samples. UvM and A.S wrote the paper.

ACKNOWLEDGEMENTS

This work was supported by Chalmers Technical University, its Excellence Initiative Nano, and Area of Advance Health. The authors greatly acknowledge further financial support from the Kristina Stenborg foundation, the foundation for Sigurd and Elsa Goljes Minne, Apotekare Hedbergs Foundation, the King Gustav V's 80 years' foundation for founding.

COMPETING INTERESTS

The authors declare no competing interests.